



ASB 2004 Pre-Doctoral Young Scientist Award

# Rectus femoris and vastus intermedius fiber excursions predicted by three-dimensional muscle models

Silvia S. Blemker, Scott L. Delp\*

*Departments of Bioengineering and Mechanical Engineering, James H. Clark Center, Room S-321, Stanford University,  
MailCode: 5450, 318 Campus Drive, Stanford, CA 94305-5450, USA*

Accepted 18 April 2005

---

**Abstract**

Computer models of the musculoskeletal system frequently represent the force–length behavior of muscle with a lumped-parameter model. Lumped-parameter models use simple geometric shapes to characterize the arrangement of muscle fibers and tendon; this may inaccurately represent changes in fiber length and the resulting force–length behavior, especially for muscles with complex architecture. The purpose of this study was to determine the extent to which the complex features of the rectus femoris and vastus intermedius architectures affect the fiber changes in length (“fiber excursions”). We created three-dimensional finite-element models of the rectus femoris and vastus intermedius muscles based on magnetic resonance (MR) images, and compared the fiber excursions predicted by the finite-element models with fiber excursions predicted by lumped-parameter models of these muscles. The finite-element models predicted rectus femoris fiber excursions (over a 100° range of knee flexion) that varied from 55% to 70% of the excursion of the muscle–tendon unit and vastus intermedius fiber excursions that varied from 55% to 98% of the excursion muscle–tendon unit. In contrast, the lumped-parameter model of the rectus femoris predicted fiber excursions that were 86% of the excursion of the muscle–tendon unit and vastus intermedius fiber excursions that were 97% of the excursion of the muscle–tendon unit. These results suggest that fiber excursions of many fibers are overestimated in lumped-parameter models of these muscles. These new representations of muscle architecture can improve the accuracy of computer simulations of movement and provide insight into muscle design.

© 2005 Elsevier Ltd. All rights reserved.

*Keywords:* Skeletal muscle; Finite-element modeling; Muscle architecture; Lower limb; Fascicle geometry; Rectus femoris; Quadriceps

---

**1. Introduction**

The organization of muscle fibers and tendon in a muscle–tendon complex (i.e., muscle–tendon architecture) greatly influences a muscle’s ability to generate force and actuate movement. To incorporate the effects of architecture, models generally represent the length of the muscle fibers, the length of the tendon, the orientation of the fibers with respect to the tendon, and the physiological cross-sectional area of the muscle

(Zajac, 1989). These “lumped-parameter” models frequently assume that fibers have an idealized two-dimensional geometrical arrangement (Fig. 1), that all fibers have the same length, that all fibers shorten by the same amount, and that the aponeurosis has the same properties and behavior as the external tendon. While lumped-parameter models have been useful for a broad range of applications in biomechanics, simplified representations of muscle architecture may be limited in their ability to characterize the *in vivo* behavior of some muscles with complex architecture.

Previous studies have shown that lumped-parameter models may not predict muscle forces that match *in vivo* experimental measurements under some circumstances.

---

\*Corresponding author. Tel.: +1 650 723 1230;  
fax: +1 650 724 1922.

*E-mail address:* [delp@stanford.edu](mailto:delp@stanford.edu) (S.L. Delp).

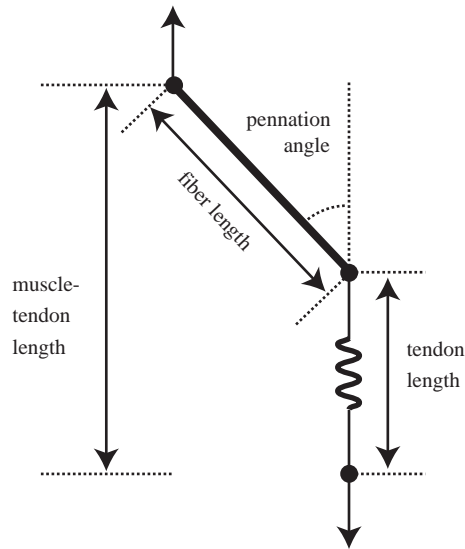


Fig. 1. Simplified, two-dimensional representation of muscle architecture commonly used in models of the musculoskeletal system. This model represents the tendon length, the muscle–fiber length, and the pennation angle.

Herzog and ter Keurs (1988) demonstrated that a lumped-parameter model of the rectus femoris predicted substantially more variation in force with knee angle than muscle forces determined from *in vivo* measurements. Van den Bogert et al. (1998) highlighted the difficulty of faithfully reproducing experimental joint moments with lumped-parameter models, in part because lumped-parameter models predict too much variation in force with change in joint angle, especially for muscles with complex architecture.

The quadriceps muscles have complex architectures. The fibers of the rectus femoris muscle follow three-dimensional trajectories, and there are two long aponeuroses within the muscle (Fig. 2A). The vastus intermedius (Fig. 2B) has a long distal aponeurosis, and, on the proximal end, all of the fibers attach directly to the femur. How might the three-dimensional trajectories of the fibers affect the muscle behavior? Do the aponeuroses behave differently from the external tendon, and how might this affect the behavior of the muscle fibers? To answer these questions, a model that incorporates the three-dimensional trajectories of the muscle fibers and the constitutive properties of muscle, aponeurosis, and tendon is needed.

The purpose of this study was to determine the extent to which the complex features of the rectus femoris and vastus intermedius architectures affect the fiber excursions. We created three-dimensional finite-element models of the rectus femoris and vastus intermedius muscles based on magnetic resonance (MR) images. The models represent the three-dimensional trajectories of the muscle fibers, the geometry of the associated bones, the kinematics of the knee joint, the nonlinear consti-

tutive properties of muscle, aponeuroses, and tendon, and contact between all relevant muscle, tendon, and bone structures. To evaluate the effects of the complex features of muscle architecture, we compared fiber excursions predicted by the three-dimensional models with fiber excursions predicted by lumped-parameter models of the rectus femoris and vastus intermedius muscles (Delp et al., 1990).

## 2. Methods

We reconstructed the surface geometry of the rectus femoris, vastus intermedius, aponeuroses, external tendons, and underlying bones from the MR images of a cadaver specimen (Fig. 3). Three sets of axial images and one set of sagittal spin-echo images were used to reconstruct the muscle and bone anatomy (repetition time = 400 ms, echo time = 17 ms, matrix size =  $256 \times 256$ ). The first series of axial images went from the iliac crest to just below the lesser trochanter (3-mm contiguous slices); the second axial series went from the greater trochanter to just below the knee (10-mm contiguous slices), and the third axial series went from above the knee to just below the knee (3-mm contiguous slices). The sagittal image series was acquired at the knee (3-mm contiguous slices) and used to achieve a detailed reconstruction of the joint anatomy. On each image, we manually outlined the boundaries of the structures of interest. Three-dimensional polygonal surface models were generated for each structure from the set of two-dimensional outlines (Nuages, INRIA, France).

We created solid hexahedral meshes of the muscles from the surface models using a mapping process performed in a finite-element mesh generator (TrueGrid, XYZ Scientific Applications, Livermore, CA). In this mapping process, a template mesh that is in the shape of a cube is morphed to fit the muscle surface. We have used this technique to create finite-element meshes for a variety of muscles (Blemker and Delp, 2005).

We created a representation of the three-dimensional geometry of fibers within each muscle (Fig. 4). We developed a method to map “template fiber geometries” to create each muscle’s “target fiber geometry.” The template fiber geometries are cubes, and the mapping function used in the meshing process described above is applied to the template fiber geometry to generate the target fiber geometry. We have described (Blemker and Delp, 2005) our methods for mapping the template fiber geometry, the basis of the templates (interpolation between rational Bezier spline curves), and the template fiber geometries for parallel, pennate, and fanned muscles. For the vastus intermedius, we used the pennate fiber geometry template (Fig. 4D), identified the origin and insertion areas of the fibers (Fig. 4E), and mapped the template to the vastus intermedius

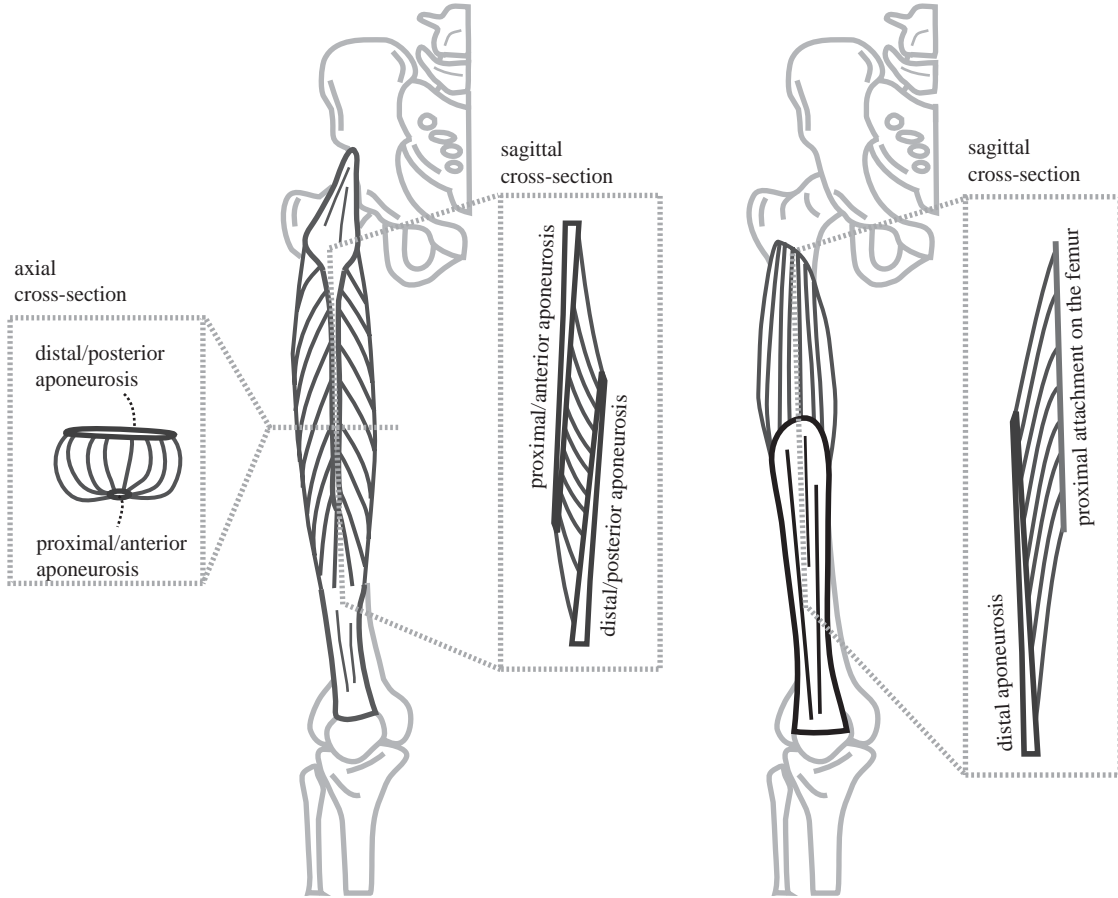


Fig. 2. Rectus femoris (left) and vastus intermedius (right) anatomy and architecture.

geometry, creating a three-dimensional representation of the muscle's fiber geometry (Fig. 4F). In the present study, we introduce a new template for the bipennate fiber geometry of the rectus femoris (Fig. 4A), which is more complex than the previously described templates. We interpolated between six sets of spline curves to define a template that characterized all possible fibers that originate on the proximal aponeurosis/tendon and insert on the distal aponeurosis/tendon. The corresponding origin and insertion areas were identified (Fig. 4B), and the template was mapped to the muscle geometry (Fig. 4C). We used the fiber geometry descriptions to define the fiber direction for each element in the mesh, which served as input to the transversely isotropic constitutive model (described below). Additionally, we sampled the fiber geometry in several locations to obtain representative “fibers” that we could track throughout a simulation to calculate fiber lengths as a function of knee flexion angle.

A nonlinear constitutive model was used to describe the stress–strain relationship for muscle and tendon tissue (see Blemker et al., 2005 for details). The model represents muscle as a quasi-incompressible, fiber-reinforced composite with transversely isotropic material

symmetry (Weiss et al., 1996); the strain energy function ( $\Psi$ ) was defined as

$$\Psi(B_1, B_2, \lambda, a, J) = W_1(B_1) + W_2(B_2) + W_3(\lambda, a) + \frac{K}{2} \ln(J)^2, \quad (1)$$

where  $a$  is the muscle activation level,  $K$  is the bulk modulus, and  $B_1, B_2, \lambda$ , and  $J$  represent the along-fiber shear strain, cross-fiber shear strain, along-fiber stretch, and volume strain, respectively. The functional forms for  $W_1$  and  $W_2$  adopted for our model are as follows:

$$W_1 = G_1(B_1)^2 \text{ and } W_2 = G_2(B_2)^2, \quad (2)$$

where  $G_1$  and  $G_2$  represent the effective along-fiber shear modulus and cross-fiber shear modulus, respectively. Eq. (2) were used to represent both muscle and tendon, with different values for constants  $G_1$  (5.0E2 Pa for muscle and 5.0E4 Pa for tendon) and  $G_2$  (5.0E2 Pa for muscle and 5.0E4 Pa for tendon). The functional form for  $W_3$  adopted for our model was

$$\lambda \frac{\partial W_3^{\text{muscle}}}{\partial \lambda} = \sigma_{\max} (a f_{\text{active}}^{\text{fiber}}(\lambda) + f_{\text{passive}}^{\text{fiber}}(\lambda)) \lambda / \lambda_o^{\text{fiber}}, \quad (3)$$

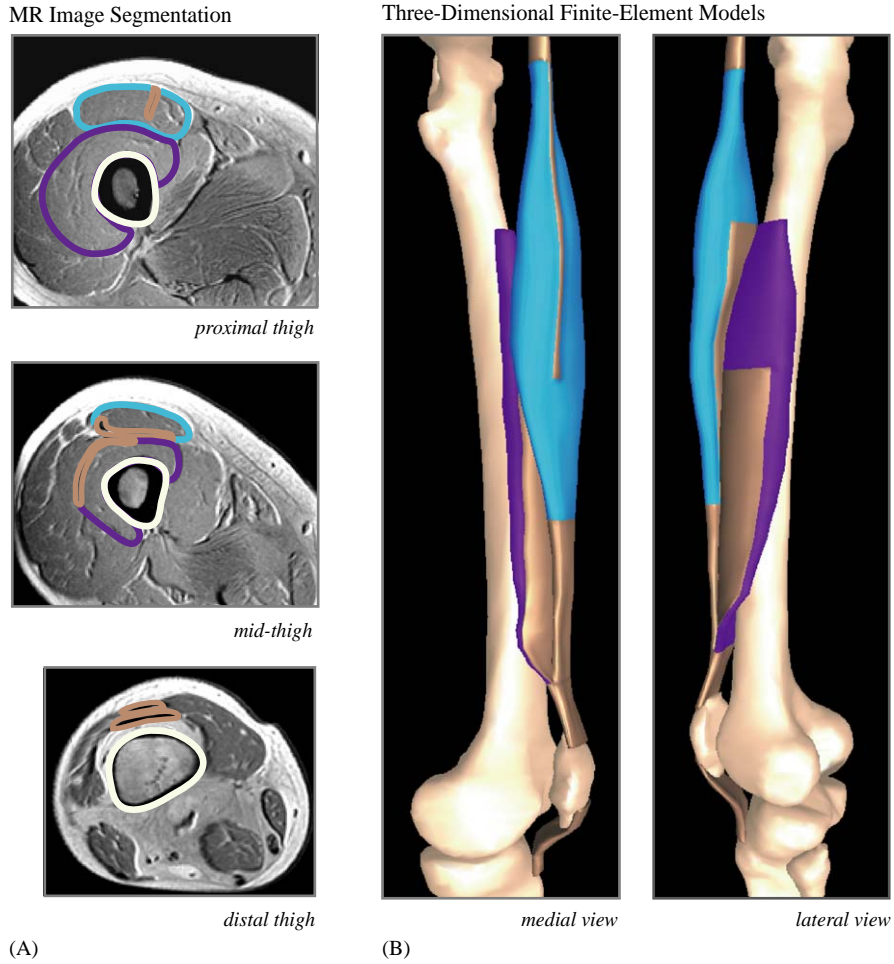


Fig. 3. (A) MR images of the proximal thigh, mid-thigh, and distal thigh with outlines of the rectus femoris (blue), vastus intermedius (purple), internal and external tendons (brown), and bones (white). (B) Three-dimensional models constructed from the outlines.

where  $\sigma_{\max}$  is the maximum isometric stress,  $\lambda_o^{\text{fiber}}$  is the fiber stretch at which the sarcomeres reach optimum length, and  $f_{\text{active}}^{\text{fiber}}$  and  $f_{\text{passive}}^{\text{fiber}}$  correspond to normalized active and passive force–length relationships of a muscle fiber (Zajac, 1989). The activation level ( $a$ ) can be any value between 0 (no activation) and 1 (maximal activation); we prescribed a value of 0.2 (20% maximum voluntary activation) for the simulation results presented in this study. We also defined  $W_3$  for tendinous tissue (i.e., external tendons and the aponeuroses) using a function that characterized the relationship between the Cauchy stress in the tendon ( $\sigma^{\text{tendon}}$ ) and the fiber stretch ( $\lambda$ ):

$$\lambda \frac{\partial W_3^{\text{tendon}}}{\partial \lambda} = \sigma^{\text{tendon}}(\lambda). \quad (4)$$

The expression for  $\sigma^{\text{tendon}}$  and the associated material constants were defined to be consistent with the stress–strain relationship for tendon (Zajac, 1989), and the same values were used for the external tendons and the aponeuroses. Strains predicted by muscle models

that use these constitutive equations match in vivo data (Blemker et al., 2005).

We performed a finite-element simulation through a range of knee flexion–extension angles. To do this, we incorporated a kinematic model that describes the three-dimensional translations and rotations of the tibia with respect to the femur as a function of knee flexion angle (Arnold et al., 2000). The femur, tibia, and patella were considered rigid bodies. A no-friction penalty contact formulation (Hallquist et al., 1985) was used to prevent penetration between the two muscles, between the muscles and the femur, and between the patella and the femur. The three-dimensional rigid body motion of the patella was resolved throughout the simulation (Puso, 2002). Quasi-static simulations were performed in NIKE3D (Puso et al., 2002), a nonlinear implicit finite-element solver. Simulation times were in the order of 15 CPU hours on a Silicon Graphics Origin 3800 shared memory super-computer (Silicon Graphics, Mountain View, CA). The results of each simulation were imported into a

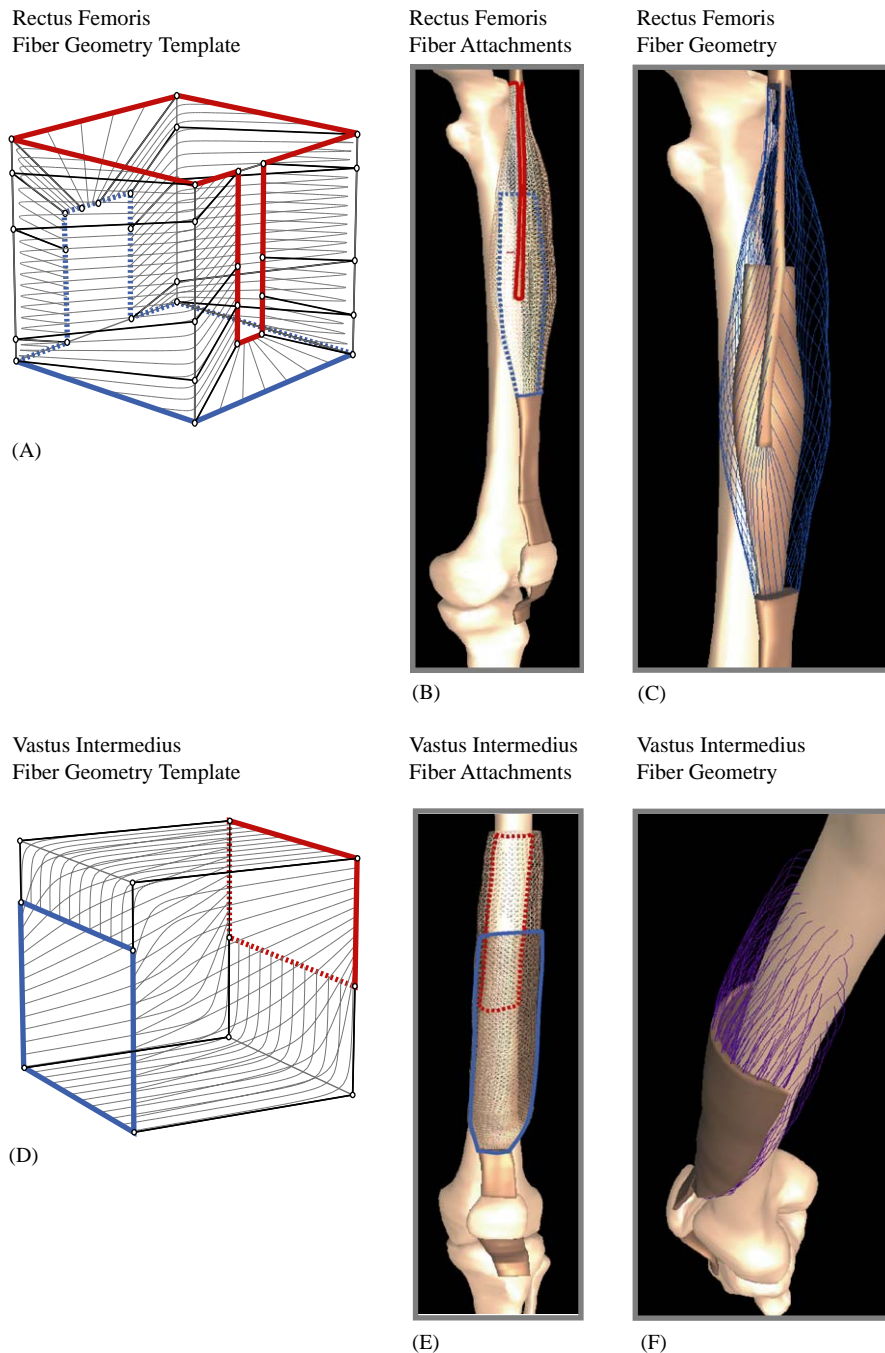


Fig. 4. Methods for representing the fiber geometries of the rectus femoris and vastus intermedius. Fiber geometry templates (A, D) were created based on a set of interpolated rational Bezier spline curves. Black straight lines and circles represent the control points for the spline curves, and the thin curved lines show representative fibers within the template. Red lines indicate the origin areas (for the rectus femoris, this includes the region of the template corresponding to the long proximal/anterior aponeurosis, and for the vastus intermedius this corresponds to the broad origin on the femur) and blue lines indicate the insertion areas (for both rectus femoris and vastus intermedius, this includes the region of the templates corresponding to the long distal aponeuroses). The corresponding areas of fiber attachments (B, E; red outlines indicate origins and blue outlines indicate insertions) were identified within the finite-element mesh, and the fiber templates (A, D) were mapped (Blemker and Delp, 2005) to fit within the finite-element mesh, creating a three-dimensional representation of each muscle's internal architecture (C, F).

graphics-based musculoskeletal modeling environment (Delp and Loan, 2000).

We calculated the muscle–tendon moment arms of the rectus femoris and vastus intermedius by defining centerline paths for each muscle–tendon unit and

calculating the length of each path throughout the simulated knee flexion. Fourth-order polynomials were fit to these data describing muscle–tendon lengths ( $\ell_{3D}^{mt}$ ) as a function of knee flexion angle ( $\theta$ ). Muscle–tendon moment arms ( $ma_{3D}^{mt}$ ) were calculated according to the

principal of virtual work (An et al., 1984):

$$\text{ma}_{3\text{D}}^{\text{mt}} = \partial \ell_{3\text{D}}^{\text{mt}} / \partial \theta, \quad (5)$$

and compared to previously reported moment arms (Buford et al., 1997). We also calculated the muscle–belly lengths ( $\ell_{3\text{D}}^{\text{belly}}$ ; portion of the muscle–tendon unit that does not include external tendon), the external tendons lengths ( $\ell_{3\text{D}}^{\text{E tendon}}$ ), the aponeurosis lengths ( $\ell_{3\text{D}}^{\text{apon}}$ ), and the fiber lengths ( $\ell_{3\text{D}}^{\text{fibers}}$ ) as a function of knee flexion angle. Fiber excursions ( $\Delta \ell_{3\text{D}}^{\text{fibers}}$ ) were calculated as the change in length (from full extension to 100° of knee flexion) of the muscle fibers. We also examined the fiber excursions normalized by the maximum excursion of the muscle–tendon unit:

$$\tilde{\Delta} \ell_{3\text{D}}^{\text{fibers}} = \Delta \ell_{3\text{D}}^{\text{fibers}} / \Delta \ell_{3\text{D}}^{\text{mt}}{}^{\text{max}}. \quad (6)$$

This unitless quantity provides an estimate of how much of the total muscle–tendon excursion is taken up by the muscle fibers and allows us to compare the fiber excursions across muscles (and models) that have different muscle–tendon moment arms.

We compared the fiber excursions predicted by the three-dimensional model with fiber excursions predicted by a four-parameter representation of muscle (Zajac, 1989), with the rectus femoris and vastus intermedius muscle–tendon parameters and musculoskeletal geometry described by Delp et al. (1990) and an activation level of 20%. This model predicts the muscle–tendon length ( $\ell_{\text{lumped}}^{\text{mt}}$ ), fiber length ( $\ell_{\text{lumped}}^{\text{fibers}}$ ), and tendon length ( $\ell_{\text{lumped}}^{\text{tendon}}$ ) as a function of knee flexion angle. The representation considers all tendon tissues as one lumped structure (i.e., the tendon length includes both the external tendon and the aponeurosis). Based on the ratio of the aponeurosis length to the total tendon length ( $\gamma_{\text{tendon}}^{\text{apon}}$ ) determined from the three-dimensional models, we calculated the aponeurosis length in the lumped-parameter models:  $\ell_{\text{lumped}}^{\text{apon}} = \gamma_{\text{tendon}}^{\text{apon}} \ell_{\text{lumped}}^{\text{tendon}}$ . The length of the muscle belly was calculated as:

$$\ell_{\text{lumped}}^{\text{belly}} = \ell_{\text{lumped}}^{\text{apon}} + \ell_{\text{lumped}}^{\text{fibers}} \cos(\alpha), \quad (7)$$

where  $\alpha$  is the pennation angle. Fiber excursions ( $\Delta \ell_{\text{lumped}}^{\text{fibers}}$ ) were calculated as the change in length (from full extension to 100° of knee flexion) of the muscle fibers, and the fiber excursions normalized by the maximum excursion of the muscle–tendon unit were calculated as:

$$\tilde{\Delta} \ell_{\text{lumped}}^{\text{fibers}} = \Delta \ell_{\text{lumped}}^{\text{fibers}} / \Delta \ell_{\text{lumped}}^{\text{mt}}{}^{\text{max}}. \quad (8)$$

### 3. Results

The peak knee extension moment arms predicted by the three-dimensional model were 3.5 cm for the rectus femoris (Fig. 5C) and 3.3 cm for the vastus intermedius

(Fig. 5D). These values are consistent with previously reported moment arms (Buford et al., 1997). This favorable comparison suggests that the muscle–tendon length changes predicted by the three-dimensional model are accurate.

The excursions of the fibers within the three-dimensional model of the rectus femoris varied across the muscle, ranging from 3.1 to 4.0 cm. These excursions correspond to 55–70% of the excursion of the whole muscle–tendon unit (Fig. 6A). The proximal aponeurosis of the rectus femoris changed length by 1.6 cm (9%), the distal aponeurosis changed length by 0.7 cm (4%), and the external tendon changed length by 0.4 cm (3%). The excursions of the vastus intermedius fibers varied substantially across the muscle, ranging from 2.7 to 4.7 cm. These excursions correspond to 55–98% of the excursion of the whole muscle–tendon unit (Fig. 6C). The aponeurosis of the vastus intermedius changed length by 1.8 cm (10%), and the external tendon changed length by 0.3 cm (1%).

The lumped-parameter model predicted fiber excursions that were larger than those predicted by the three-dimensional model. For the rectus femoris (Fig. 6B), the lumped-parameter model predicted fiber excursions that were 86% of the excursion of the whole muscle–tendon unit. For the vastus intermedius (Fig. 6D), the lumped parameter model predicted fiber excursions that were 97% of the excursion of the whole muscle–tendon unit.

### 4. Discussion

The three-dimensional models of the rectus femoris and vastus intermedius presented in this paper indicate that the complex architecture of these muscles substantially affects the excursions of the muscle fibers. The fiber excursions were affected in two ways. Firstly, the excursions varied across fibers within the muscles, suggesting that the assumption made in lumped-parameter models that all muscle fibers shorten by the same amount may be invalid for the rectus femoris and vastus intermedius muscles. Secondly, the fiber excursions predicted by the three-dimensional models were on average substantially less than those predicted by the lumped-parameter models.

How do these differences in muscle–fiber excursions affect the force–length behavior? The ratio of the fiber excursion to the optimal fiber length ( $\Delta \ell^{\text{fibers}} / \ell_0^{\text{fibers}}$ ) is a metric of the fiber's operating range on the muscle force–length curve (Hoy et al., 1990). We determined these ratios by dividing the fiber excursions by optimal fiber lengths derived from Wickiewicz et al. (1983). In this context, we calculated the ratio as  $\tilde{\Delta} \ell_{\text{lumped}}^{\text{fibers}} \Delta \ell_{\text{lumped}}^{\text{mt}} / \ell_0^{\text{fibers}}$  for the lumped-parameter model and  $\tilde{\Delta} \ell_{3\text{D}}^{\text{fibers}} \Delta \ell_{3\text{D}}^{\text{mt}} / \ell_0^{\text{fibers}}$  for the three-dimensional

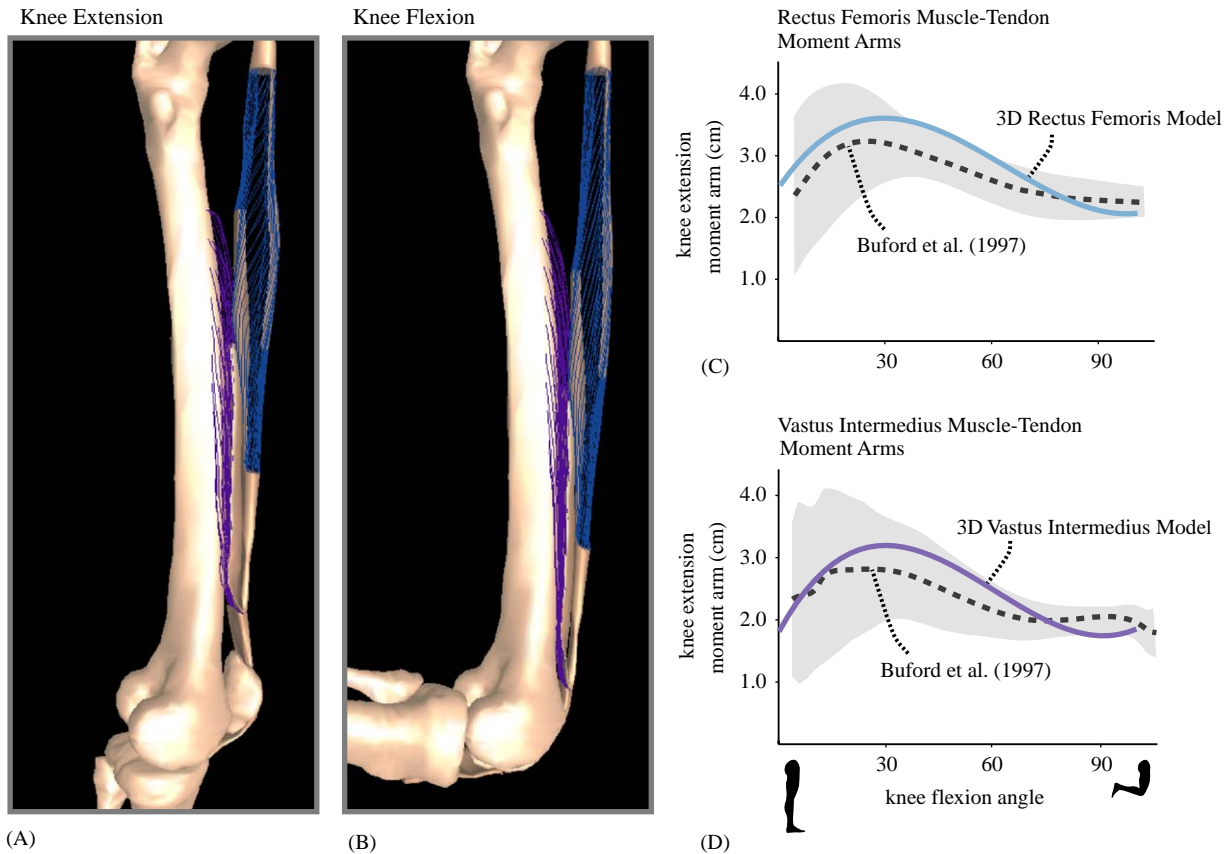


Fig. 5. Rectus femoris and vastus intermedius model results in the knee extended (A) and flexed (B) and muscle–tendon knee extension moment arms for the rectus femoris (C) and vastus intermedius (D). The moment arms are compared with Buford et al. (1997) (dotted lines correspond to the average values from 15 cadaveric specimens; shaded regions correspond to  $\pm$  one standard deviation).

model. The same muscle–tendon excursions ( $\Delta \ell_{\text{lumped}}^{\text{mt}}$ ) were used to eliminate the effects of differences in muscle–tendon moment arms between the lumped-parameter and three-dimensional models. For the three-dimensional model of the vastus intermedius, the ratio varied across muscle fibers from 0.41 to 0.73 (Fig. 7). By contrast, all of the fibers in the lumped parameter of the vastus intermedius had the same ratio of 0.73. The rectus femoris had a similar behavior—the ratio of fiber excursion to optimal fiber length varied from 0.46 to 0.59 for the three-dimensional model, but had a single value of 0.73 for the lumped-parameter model. These results indicate that the complex fiber and tendon geometry causes many of the fibers to operate over a smaller range of the force–length curve, which would result in less variation in muscle force with joint angle.

For both muscles, the aponeurosis strains were substantially higher than the external tendon strains. The higher strains in the aponeuroses affected the rectus femoris and vastus intermedius fiber excursions. The proximal fibers of the vastus intermedius have more in-series tendon than the distal fibers (Fig. 2B); the stretch of the long aponeurosis resulted in high variability of excursions across the vastus intermedius fibers. The

variation in excursions of the rectus femoris fibers is a consequence of the different dimensions (and different changes in length) between the muscle’s two aponeuroses. These results highlight the importance of the aponeurosis in the in vivo function of muscles.

The findings from our simulations are similar to experimental studies. In vivo measurements of muscle and tendon tissue have shown that the changes in length of muscle fascicles and tendons may be different from those predicted by simplified models of muscle architecture. Imaging measurements have shown that muscle fascicle excursions are different from model predictions (Herbert et al., 2002), aponeurosis strains are different from the strains in the external tendon (Muramatsu et al., 2002), and different fascicles within the same muscle undergo different changes in length (Pappas et al., 2002).

Previous models have also suggested that complex features of muscle architecture can affect the behavior of muscle fibers. For example, models that introduce specific complexities, such as variations in fiber lengths (Ettema and Huijing, 1994), aponeurosis stretch (Zuurbier and Huijing, 1992), and fiber curvature (Otten, 1988) have shown that each of these factors can potentially

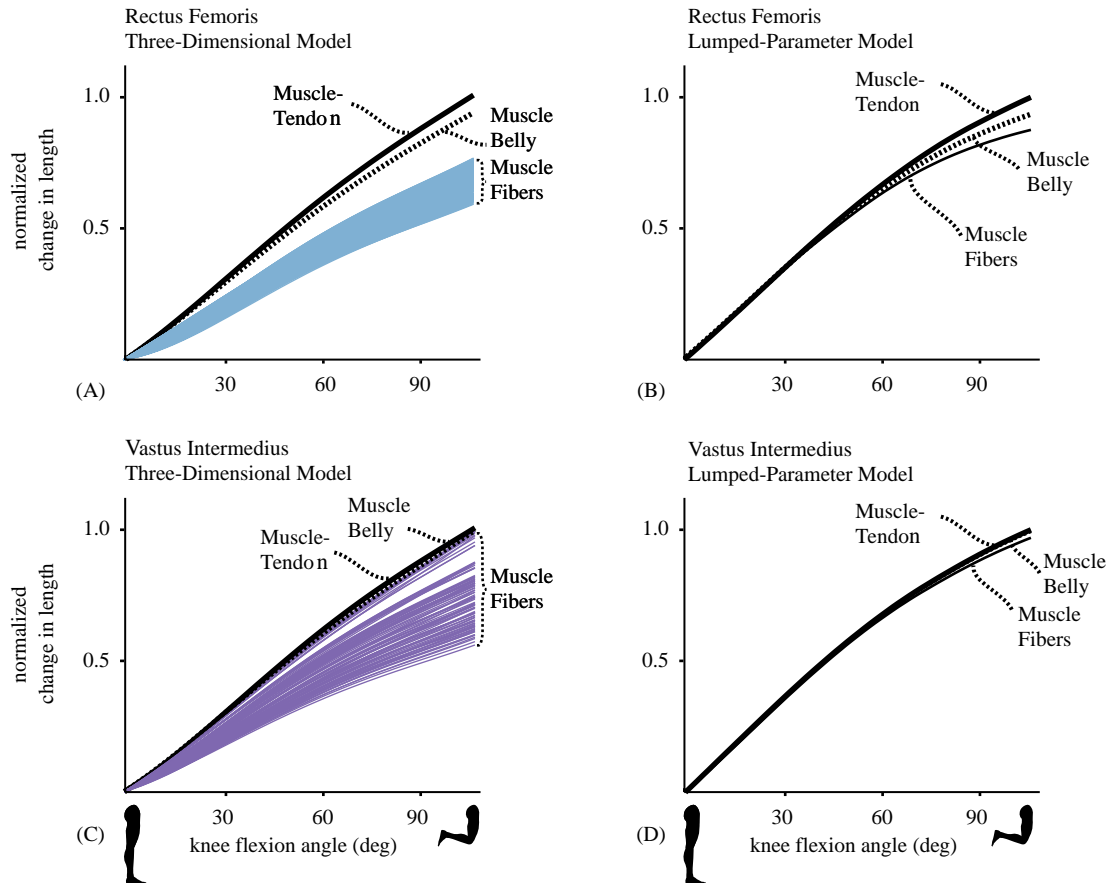


Fig. 6. Rectus femoris and vastus intermedius muscle–tendon, muscle–belly, and muscle–fiber changes in length (“excursion”) with knee flexion predicted by the three-dimensional model (A, C) are compared to those predicted by the lumped-parameter model (B, D). Excursions are normalized to the maximum excursions of the muscle–tendon unit for the corresponding muscle and model. The difference in excursion between the muscle–tendon unit and the muscle belly provides an estimate of the amount of total excursion taken up by the external tendon, which was similar between the three-dimensional and lumped-parameter models. The differences in the fiber excursion between the two models are due to the three-dimensional fiber geometry and the stretch in the aponeurosis.

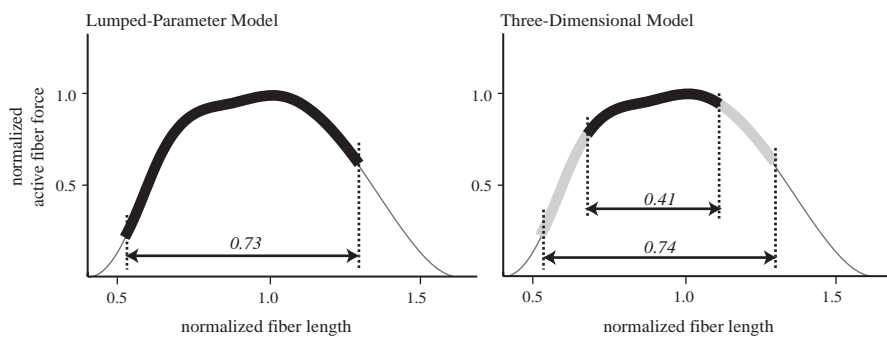


Fig. 7. Conceptual illustration of how the ratios of fiber excursions to optimal fiber lengths ( $\Delta \ell^{\text{fibers}} / \ell_0^{\text{fibers}}$ ) may affect the force–length behavior of muscle. These ratios define the range of the normalized force–length curve over which the fibers operate, illustrated here as thick lines superimposed on normalized force–length curves (thin lines). For the vastus intermedius muscle, shown here, the lumped-parameter model (left) predicts that all the fibers have the same ratio of 0.73 (thick black line), which results in substantial variation in active muscle force. In contrast, the fibers in the three-dimensional models (right) have ratios varying from 0.74 (thick gray line) to as low as 0.41 (thick black line), which would result in less variation in active muscle force than predicted by the lumped-parameter model.

affect the force–length behavior of a single muscle. Other modeling approaches have included extra parameters into the lumped-parameter models that char-

acterize effects such as length-dependence of activation (Huijing, 1996) and to systematically vary muscle–tendon parameters to match the lumped-parameter model

predictions with experimental data (Lloyd and Besier, 2003). Our study augments previous modeling work by investigating the behavior of fibers in the context of realistic, three-dimensional, mechanics-based representations of muscle. By using three-dimensional models to investigate the fiber behaviors of a variety of muscles, we could propose additional parameters that could augment lumped-parameter model and improve their ability to represent muscles with complex architectures.

The representations of muscle presented in this paper, which capture the effects of complex features of muscle architecture, can improve the accuracy of computer simulations of movement that are used for a wide variety of applications. Muscle fascicle arrangements vary widely across muscle architectures (Alexander and Ker, 1990). The modeling framework presented here provides a new paradigm for exploring how wide variations in the design of muscles influence their capacity to actuate movement.

### Acknowledgments

We are thankful to Garry Gold, Allison Arnold, the Lawrence Livermore National Labs, and the Stanford Bio-X supercomputer facility. Funding for this work was provided by the National Institutes of Health Grants HD38962, HD33929, and 1-U54-GM072970, and a Stanford Bio-X IIP Grant.

### References

- Alexander, R.M., Ker, R.F., 1990. The architecture of leg muscles. In: Winters, J.M., Woo, S.L. (Eds.), *Multiple Muscle Systems*, pp. 568–577.
- An, K.N., Takahashi, K., Harrigan, T.P., Chao, E.Y., 1984. Determination of muscle orientations and moment arms. *Journal of Biomechanical Engineering* 106, 280–282.
- Arnold, A.S., Salinas, S., Asakawa, D.J., Delp, S.L., 2000. Accuracy of muscle moment arms estimated from MRI-based musculoskeletal models of the lower extremity. *Computer Aided Surgery* 5, 108–119.
- Blemker, S.S., Delp, S.L., 2005. Three-dimensional representation of complex muscle architectures and geometries. *Annals of Biomedical Engineering* 33, 662–674.
- Blemker, S.S., Pinsky, P.M., Delp, S.L., 2005. A 3D model of muscle reveals the causes of nonuniform strains in the biceps brachii. *Journal of Biomechanics* 38, 657–665.
- Buford, W.L., Ivey, F.M., Malone, J.D., Patterson, R.M., Peare, G.L., Nguyen, D.K., Stewart, A.A., 1997. Muscle balance at the knee—moment arms for the normal knee and the ACL-minus knee. *IEEE Transactions on Rehabilitation Engineering* 5, 367–379.
- Delp, S.L., Loan, J.P., 2000. A computational framework for simulation and analysis of human and animal movement. *IEEE Computing in Science and Engineering* 2, 46–55.
- Delp, S.L., Loan, J.P., Hoy, M.G., Zajac, F.E., Topp, E.L., Rosen, J.M., 1990. An interactive graphics-based model of the lower extremity to study orthopaedic surgical procedures. *IEEE Transactions on Biomedical Engineering* 37, 757–767.
- Ettema, G.J., Huijting, P.A., 1994. Effects of distribution of muscle fiber length on active length-force characteristics of rat gastrocnemius medialis. *Anatomical Record* 239, 414–420.
- Hallquist, J.O., Goudreau, G.L., Bension, D.J., 1985. Sliding interfaces with contact-impact in large-scale lagrangian computations. *International Journal for Numerical Methods in Engineering* 51, 107–137.
- Herbert, R.D., Moseley, A.M., Butler, J.E., Gandevia, S.C., 2002. Change in length of relaxed muscle fascicles and tendons with knee and ankle movement in humans. *Journal of Physiology* 539, 637–645.
- Herzog, W., ter Keurs, H.E., 1988. Force-length relation of in-vivo human rectus femoris muscles. *Pflügers Archiv* 411, 642–647.
- Hoy, M.G., Zajac, F.E., Gordon, M.E., 1990. A musculoskeletal model of the human lower extremity: the effect of muscle, tendon, and moment arm on the moment-angle relationship of musculotendon actuators at the hip, knee, and ankle. *Journal of Biomechanics* 23, 157–169.
- Huijting, P.A., 1996. Important experimental factors for skeletal muscle modelling: non-linear changes of muscle length force characteristics as a function of degree of activity. *European Journal of Morphology* 34, 47–54.
- Lloyd, D.G., Besier, T.F., 2003. An EMG-driven musculoskeletal model to estimate muscle forces and knee joint moments in vivo. *Journal of Biomechanics* 36, 765–776.
- Muramatsu, T., Muraoka, T., Kawakami, Y., Fukunaga, T., 2002. Superficial aponeurosis of human gastrocnemius is elongated during contraction: implications for modeling muscle-tendon unit. *Journal of Biomechanics* 35, 217–223.
- Otten, E., 1988. Concepts and models of functional architecture in skeletal muscle. *Exercise & Sport Sciences Reviews* 16, 89–137.
- Pappas, G.P., Asakawa, D.S., Delp, S.L., Zajac, F.E., Drace, J.E., 2002. Nonuniform shortening in the biceps brachii during elbow flexion. *Journal of Applied Physiology* 92, 2381–2389.
- Puso, M.A., 2002. An energy and momentum conserving method for rigid-flexible body dynamics. *International Journal for Numerical Methods in Engineering* 53, 1393–1414.
- Puso, M.A., Maker, B.N., Ferencz, R.M., Hallquist, J.O., 2002. Nike3d: a nonlinear, implicit, three-dimensional finite element code for solid and structural mechanics. Lawrence Livermore National Lab Technical Report, UCRL-MA-105268.
- van den Bogert, A.J., Gerritsen, K.G., Cole, G.K., 1998. Human muscle modelling from a user's perspective. *Journal of Electromyography and Kinesiology* 8, 119–124.
- Weiss, J.A., Maker, B.N., Govindjee, S., 1996. Finite element implementation of incompressible, transversely isotropic hyperelasticity. *Computer Methods in Applied Mechanics and Engineering* 135, 107–128.
- Wickiewicz, T.L., Roy, R.R., Powell, P.L., Edgerton, V.R., 1983. Muscle architecture of the human lower limb. *Clinical Orthopaedics and Related Research* 179, 275–283.
- Zajac, F.E., 1989. Muscle and tendon: properties, models, scaling, and application to biomechanics and motor control. *Critical Reviews in Biomedical Engineering* 17, 359–411.
- Zuurbier, C.J., Huijting, P.A., 1992. Influence of muscle geometry on shortening speed of fibre, aponeurosis and muscle. *Journal of Biomechanics* 25, 1017–1026.